2001

Lagrangian flow in the California Undercurrent, an observation and model comparis

Garfield, Newell

Elsevier

Journal of Marine Systems, 29, (2001, pp. 201-220

ELSEVIER

Journal of Marine Systems 29 (2001) 201–220

JOURNAL OF MARINE SYSTEMS

www.elsevier.nl/locate/jmarsys

Lagrangian flow in the California Undercurrent, an observation and model comparison

Newell Garfield [a,*], Mathew E. Maltrud [b], Curtis A. Collins [c], Thomas A. Rago [c], Robert G. Paquette [c]

[a] *Romberg Tiburon Center, San Francisco State University, P.O. Box 855, Tiburon, CA 94920, USA*
[b] *Los Alamos National Laboratory, Los Alamos, NM, USA*
[c] *Department of Oceanography, Naval Postgraduate School, Monterey, CA, USA*

Received 31 October 1999; accepted 14 September 2000

Abstract

During the period 1992–1998, 38 isobaric RAFOS floats were deployed to sample the subsurface flow of the California Undercurrent. The deployments, released over the California continental slope west of San Francisco, have sampled robust year-round poleward subsurface flow associated with the Undercurrent most seasons and the combined inshore current and Undercurrent in winter. Two other types of flow have been seen: a region of weak flow with little net displacement just west of the California Undercurrent, and an active westward propagating eddy field. This eddy field appears to be the primary mechanism for moving floats from the Undercurrent into the ocean interior. The observations and statistics from the RAFOS floats are compared with Lagrangian estimates of particles tracked in a global high resolution ocean simulation in order to evaluate the fidelity of the model along an eastern boundary. The results show that the model reproduces the general character of the flow reasonably well, but underestimates both the mean and eddy energies by a substantial amount. © 2001 Published by Elsevier Science B.V.

Keywords: Lagrangian flow; California Undercurrent; Eddy field

1. Introduction

As numerical ocean circulation models reach higher and higher spatial resolution it becomes increasingly important to compare them with all kinds of observations including Lagrangian floats. Initially, as in this paper, these comparisons are approached from a model validation point of view. We compare RAFOS float trajectories with the output from a high resolution (1/5° on average) almost-global simulation of the Parallel Ocean Program (POP). Although POP is formulated in an Eulerian framework and most of the model/data comparisons performed with it have been with Eulerian data sources, such as satellite altimeters and moorings (see Maltrud et al., 1998), the model has the ability to simulate Lagrangian data as well. Both flow patterns (trajecto-

* Corresponding author. Fax: +1-415-435-7120.
E-mail address: garfield@sfsu.edu (N. Garfield).

0924-7963/01/$ - see front matter © 2001 Published by Elsevier Science B.V.
PII: S0924-7963(01)00017-3

ries) and statistics from the model Lagrangian motion are compared with the RAFOS observations. This represents one of the first comparisons between the model and subsurface Lagrangian observations.

The California Current System (CCS) consists of three main currents (see Hickey, 1998, for a recent review): the equatorward flowing California Current, and two poleward flowing inshore currents known as the Davidson Current and the California Undercurrent (CUC). The California Current is a shallow surface flow which is centered about 300 km offshore from Monterey and is easily distinguished as a surface lens of fresh (salinity = 32.8) water. It appears strongest in the spring. Off Monterey, subsurface poleward flow (CUC) typically occurs from the shelf break to a distance of about 100 km from the shelf break (Collins et al., 2000). Although the mean subsurface flow is poleward in all months, a broad, surface-intensified poleward flow occurs in winter months off Central California and is associated with a trough in the dynamic topography, which is centered at about (123°W) at the latitude of Monterey (Lynn and Simpson, 1987; Schwing et al., 1991). Poleward flow is also observed over the upper slope during much of the year and is strongest during March–August. This system of currents is also affected by longer period variation such as interannual El Niño events (the latest occurring in 1991–1992 and 1997–1998), which result in perturbations to coastal regions that are as large as the seasonal variability. The CCS includes a complex system of eddies, filaments and jets.

Garfield et al. (1999) (henceforth GCPC99) reported on a study of the Lagrangian character of the intermediate level flow adjacent to the coast from central California to Oregon obtained by tracking neutrally buoyant subsurface RAFOS floats. This article revises and updates our description of the subsurface flow, particularly the California Undercurrent. The data are then used in a comparison of the POP model output for this region.

The previous results of GCPC99 were based upon 1900 days of RAFOS data obtained during 1992–1995. These floats, launched off San Francisco and Monterey, exhibited three patterns with their trajectories: poleward flow in the undercurrent; reversing, but predominantly alongshore, flow adjacent to the continental margin; and, farther offshore, primarily anticyclonic motion accompanied by slow westward drift. Their results also showed flow continuity of the undercurrent between Pt. Reyes and at least Cape Mendocino, with average speed dependent upon the float depth. The data set now has almost twice as many floats and thrice the number of float days than that used by GCPC99.

The remainder of this manuscript is organized as follows: (2) observational data, Lagrangian results and statistics, (3) model results, (4) discussion, and (5) summary.

2. Observational data

2.1. NPS RAFOS floats

The RAFOS float (Rossby et al., 1986) is an acoustically tracked, neutrally buoyant, subsurface Lagrangian drifter. The float electronics are contained within a glass pressure housing approximately 2 m in length, 0.1 m in diameter and weighing 15 kg. The float commonly measures temperature and pressure at fixed time intervals, and uses a hydrophone to record the arrival times of acoustic signals transmitted from moored sound sources. Recorded temperature has a resolution of 0.02°C and an accuracy of 0.05°C. Pressure has a resolution of 2.5 decibar (1 dbar = 10^4 Pa, and a change of 1 dbar is approximately a vertical change of 1 m) and an accuracy of one percent full scale. A float is preballasted for a specified pressure and remains submerged for a preprogrammed time. At the end of the subsurface mission, a ballast weight is released which allows the float to surface and to transmit the recorded data back to the user via the ARGOS satellite system. The float trajectory is computed in postprocessing using the locations of the sound sources, the float-recorded times of arrival, and sound speed values appropriate for the study area.

For this project, the Naval Postgraduate School (NPS) floats were configured as quasi-isobaric surface followers. The floats are less compressible than seawater so they have a restoring force when displaced off the target equilibrium pressure surface. Quasi-isobaric construction constrains the float to

remain near a pressure surface; it is not a 3-D particle tracker. If the water mass characteristics change, particularly temperature, the float's equilibrium depth will change.

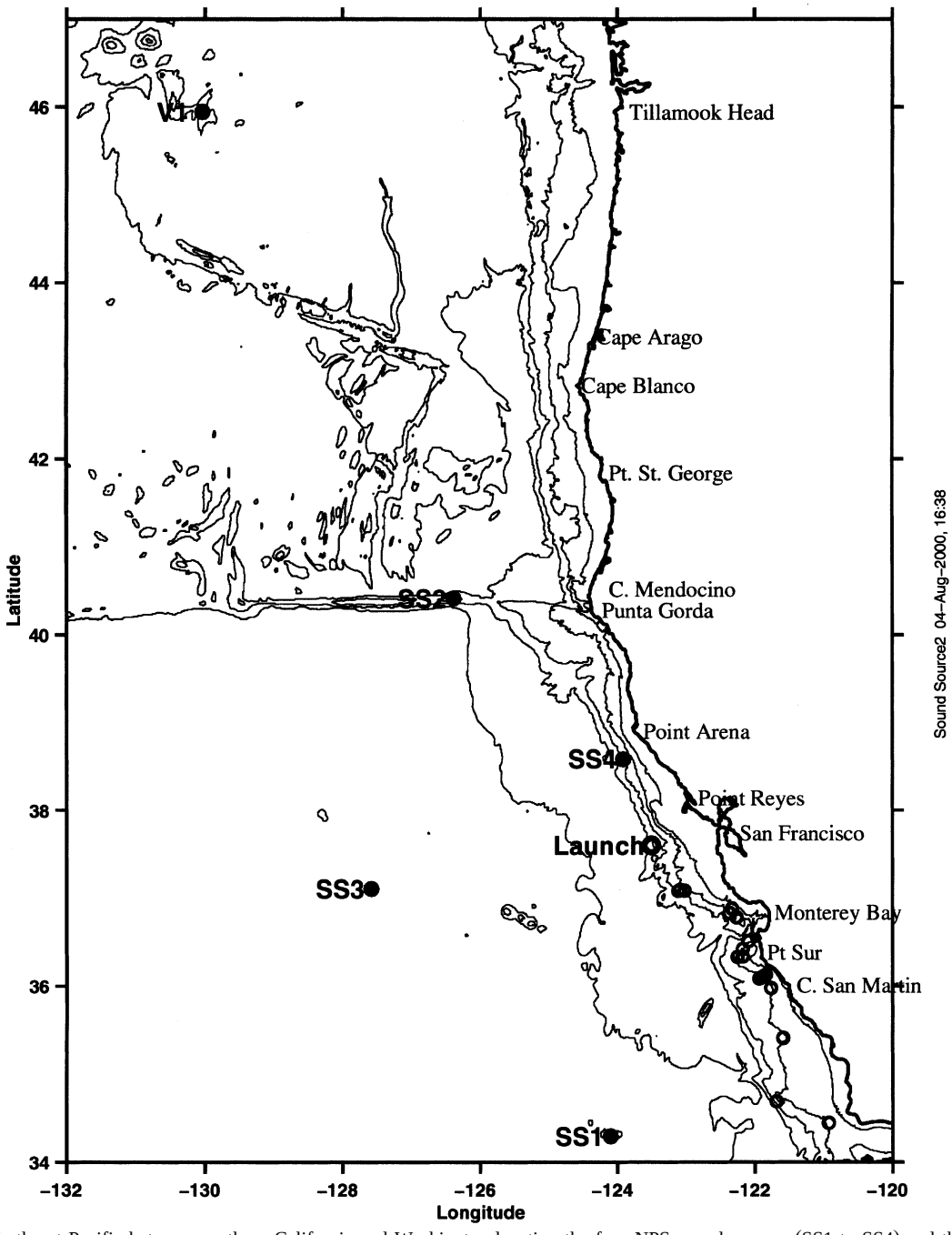

Fig. 1. Northeast Pacific between southern California and Washington locating the four NPS sound sources (SS1 to SS4) and the NOAA PMEL sound source (V1). The isobaths for 200, 1000, 2000, 3000, and 4000 m are contoured. The primary launch site is indicated by the heavy open circle west of San Francisco. Lighter circles are the locations where launches have occasionally occurred.

2.2. Field methods

An array of acoustic sound sources (Webb Research, 183-dB instruments) ensonified the region between 34°N and 46°N (Fig. 1). The sources have been deployed since 1992 (solid circles), with source turn-around cruises occurring in 1994 and 1999. Since 1994, the sources' broadcast schedules have been twice daily. The deployment depth for each sound source is at the mean depth of the deep sound channel (SOFAR channel) as reported by Johnson and Norris (1968). Sound source performance is monitored at the NPS Pt. Sur Ocean Acoustic Observatory. Both signal strength and time of arrival are recorded. Timing drift of the source signals is determined by reception at this facility and is used in the position determination for the RAFOS floats.

Float processing for position, pressure and temperature was accomplished using the procedure detailed in Paquette (1996) and GCPC99. GCPC99 analyzed the first 21 records we had obtained. Through 1998, that number has increased to 38. The number of float days has almost tripled since recent floats have had longer subsurface missions. Float deployments have continued from the primary launching region west of San Francisco, CA (37.75°N, 123.5°W), where triads of floats are deployed in a triangle 8 km to a side (heavy open circle in Fig. 1). In addition, floats have been released along the continental margin from Cape San Martin,

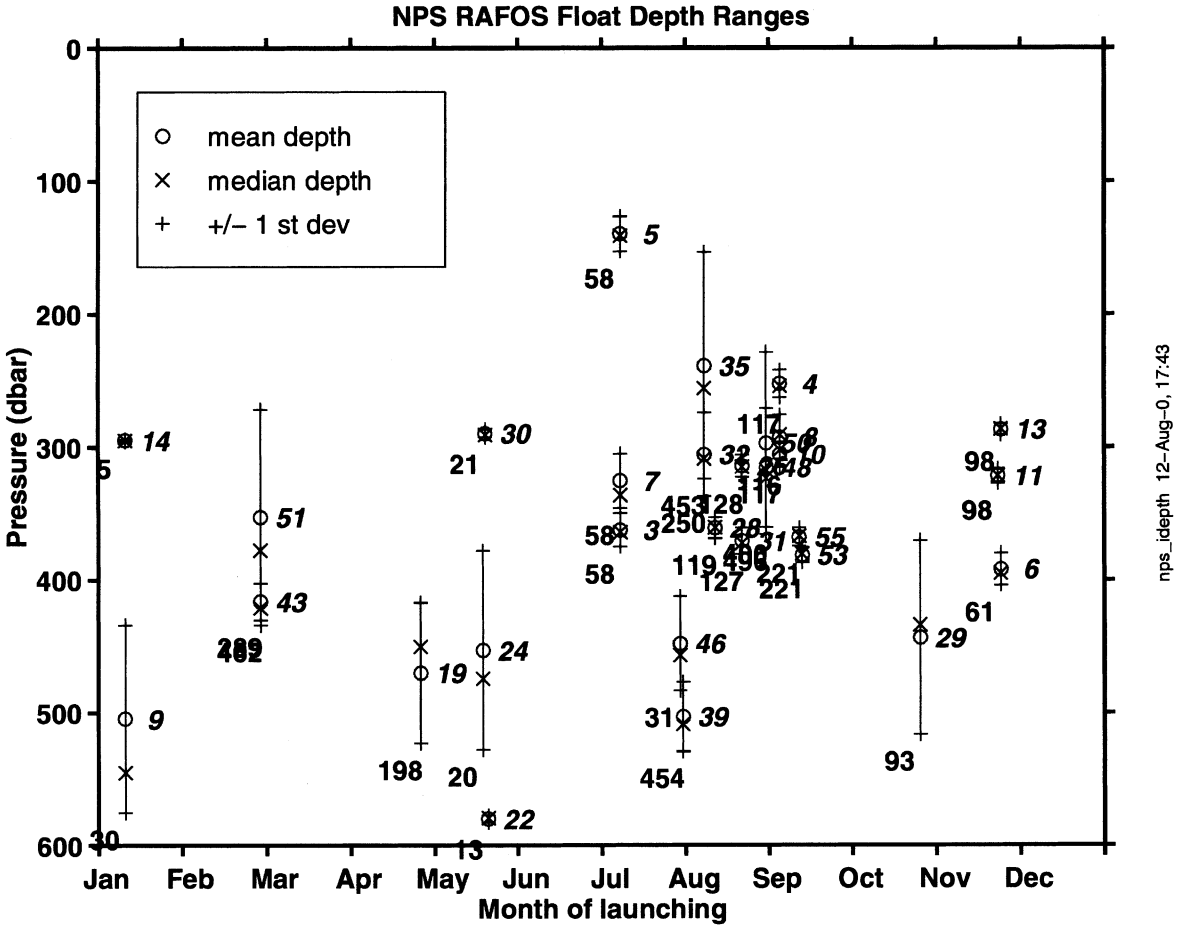

Fig. 2. Depth range (mean, median and standard deviation) of the NPS RAFOS floats. The NPS float number is in italics to the right of the mean depth, and the number of daily pressure values used to determine the statistics is below the variance bar. The depth for NPS14 was estimated from the temperature record. The depth variability is placed at the launch date for each float.

CA, northward to Pt. Reyes and San Francisco. During some cruises originating in Monterey Bay, up to three floats have been launched over the 1000 m isobath, with each float separated by about 10 km (open circles in Fig. 1). A number of deeper floats have also been launched either off the continental margin or over the Juan de Fuca and Gorda Ridges (Lupton et al., 1998).

Most of the northeast Pacific deployments have been with the specific goal of measuring the California Undercurrent. The majority of the floats have been released near the 1000 m isobath between Cape San Martin and Pt. Reyes, CA. The predetermined target depth for the floats was initially 350 m and later 270 m. The depth is a compromise between the desire to be at the depth of the Undercurrent core (approximately 100–150 m, Rischmiller, 1993; Collins et al., 2000) and the need to be deep enough to ensure good acoustic reception. The sound channel axis in the northeast Pacific is quite shallow, around 550 m (Johnson and Norris, 1968). The deployment depth was chosen to be between the core of the current and the sound channel axis.

Variation from the target depth is greater than desired. We ballast the floats at the Deep Ocean Simulation Facility, Naval Civil Engineering Laboratory, Port Hueneme, CA. The large pressure vessel, 1.9 m diameter $\times$ 3 m deep, is operated with filtered tap water rather than distilled water. Despite efforts to compensate for this water, the uncertainty has led to a standard deviation of the float target depths of $\pm$28 m. In one sense, this uncertainty has improved our experiment by allowing estimation of the vertical gradient of the California Undercurrent horizontal speed. Fig. 2 shows the mean, median and standard deviation of the depth for each float shallower than

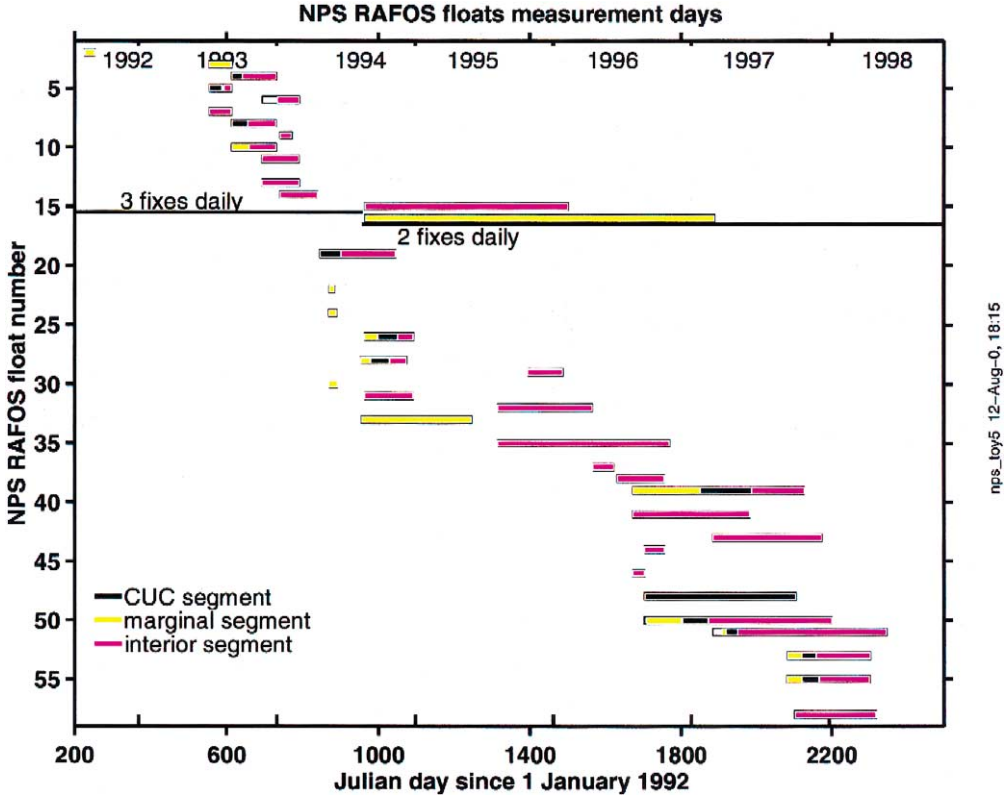

Fig. 3. Deployment schedule for the 39 floats used in this study. The shading separates the float days into the three types of observed motion. Black are the float days in the California Undercurrent, magenta are float days in the interior region, and yellow are float days for reversing marginal flow. The white region in NPS6 represents a period of unknown position.

600 m plotted by month of launch. Floats with a large standard deviation and large offset between the mean and median depth were floats that showed a depth increase during the mission, which we attribute to leakage in either the float or, for early floats, the ballast weight.

Cruises were not dedicated to float deployments; rather deployments were done as opportunity arose. Fig. 3 shows the deployment times and mission durations for the floats deployed through 1997 and with missions completed by the end of 1998. Fig. 4 shows the frequency distribution of "float days" as a function of year and month.

A "spaghetti" plot showing all the successfully navigated floats at depths less than 600 m (Fig. 5) clearly shows the poleward movement along the continental margin as well as the large number of floats which moved westward south of 40°N. North of 40°N there is also westward flow, but most of the floats that traveled north of this latitude surfaced relatively shortly after leaving the continental margin. The large concentration of float trajectories near the launch sites is due to both floats that moved very slowly, staying relatively close to the launch sites during their subsurface missions, and floats moving westward with anticyclonic eddy motion.

2.3. Eulerian statistics

In order to increase the number of degrees of freedom for statistical analyses, the float data set was "increased" by creating "pseudo" floats (Poulain and Niiler, 1989). Every 10 days, the position of a float was used as the start of a new "pseudo" float that then traveled as the parent float. The pseudo float had to have a record length exceeding 20 days to be used in the analyses. In this way, the number of "floats" was increased from 38 to 736. A more

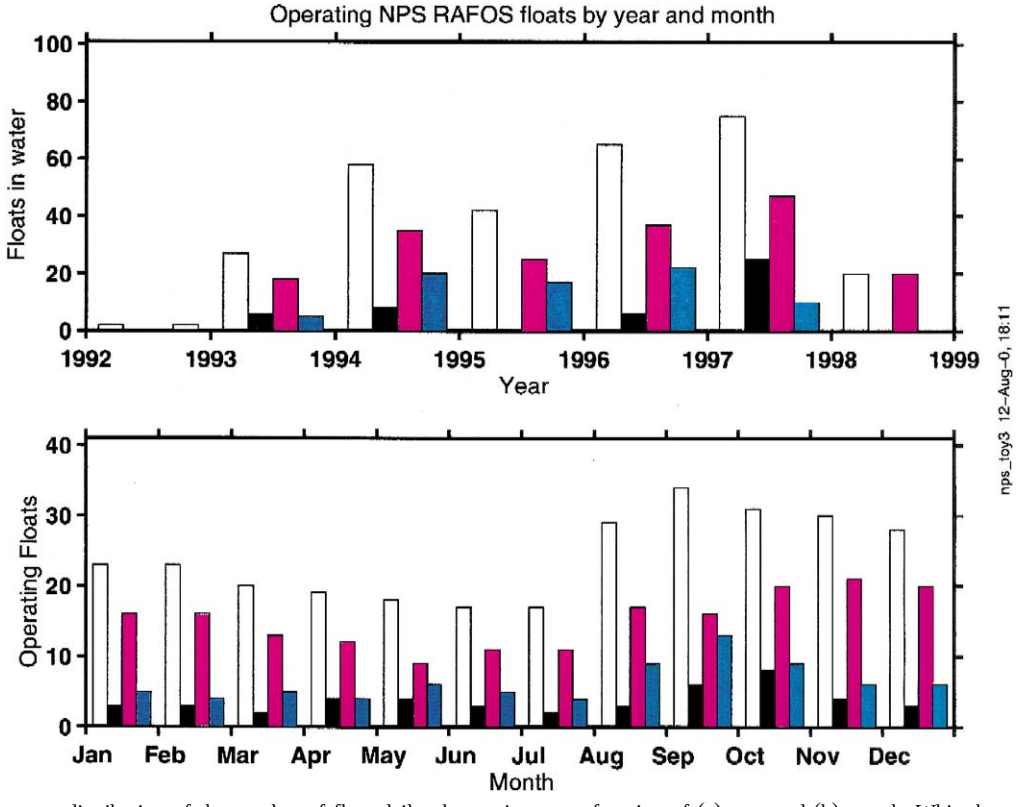

Fig. 4. Frequency distribution of the number of float daily observations as a function of (a) year and (b) month. White bars in a and b indicate the total float days for all floats and black, magenta and blue are for, respectively, the California Undercurrent, interior and marginal flow segments.

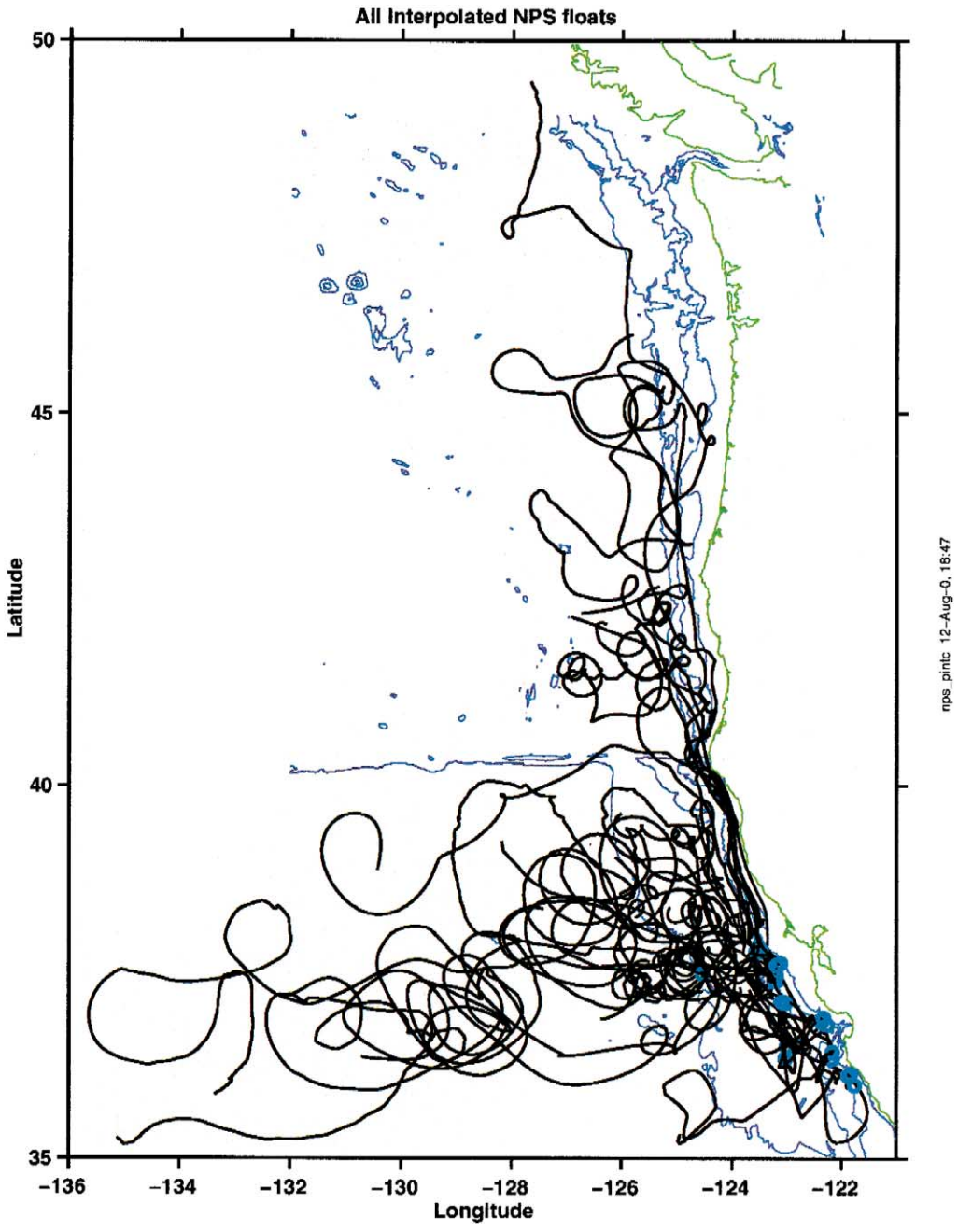

Fig. 5. Ensemble spaghetti diagram showing the smoothed subsurface trajectories of all RAFOS floats at depths less than 600 m. Launch sites are indicated by the open circles. Isobaths are shown east of 132°W for 100, 1000, 2000 and 4000 m.

complete description of this procedure is found in Poulain and Niiler and GCPC99.

The estimates of the Eulerian speed and variance were computed for the entire float data set and the three flow types discussed below in Section 2.4 (Table 1). In addition, the areal Eulerian statistics were computed by binning the float data into one degree latitude by two degree longitude bins (Fig. 6).

Table 1
Float velocity and speed statistics determined from partitioning the floats into the different types of observed flow

Type of flow	Number of floats	Pseudo floats	U mean and std. dev. (cm s^{-1})	V mean and std. dev. (cm s^{-1})	Mean speed and std. dev. (cm s^{-1})
RAFOS floats					
All	38	736	-1.1 ± 1.6	0.6 ± 1.8	6.2 ± 3.4
Undercurrent	12	74	-1.8 ± 1.8	5.7 ± 3.2	7.1 ± 3.4
Marginal	15	153	-0.1 ± 0.8	-0.2 ± 1.4	3.6 ± 1.7
Interior	30	425	-1.1 ± 1.8	0.1 ± 1.3	6.6 ± 3.6
Model floats					
All	400	–	-0.4 ± 0.2	0.7 ± 0.6	1.8 ± 0.4
Undercurrent	259	–	-0.4 ± 0.2	1.1 ± 0.3	1.9 ± 0.4
Interior	141	–	-0.4 ± 0.3	-0.1 ± 0.3	1.8 ± 0.3

A minimum of 15 observations was used in computing the binned statistics. In the offshore region, the data are sparse and often dominated by a single eddy. However, the general sense of the interior flow is westward. Along the coast, the Eulerian flow clearly shows the California Undercurrent by the alongshore mean flow and the polarized variance. Just seaward of the CUC, there is a region showing

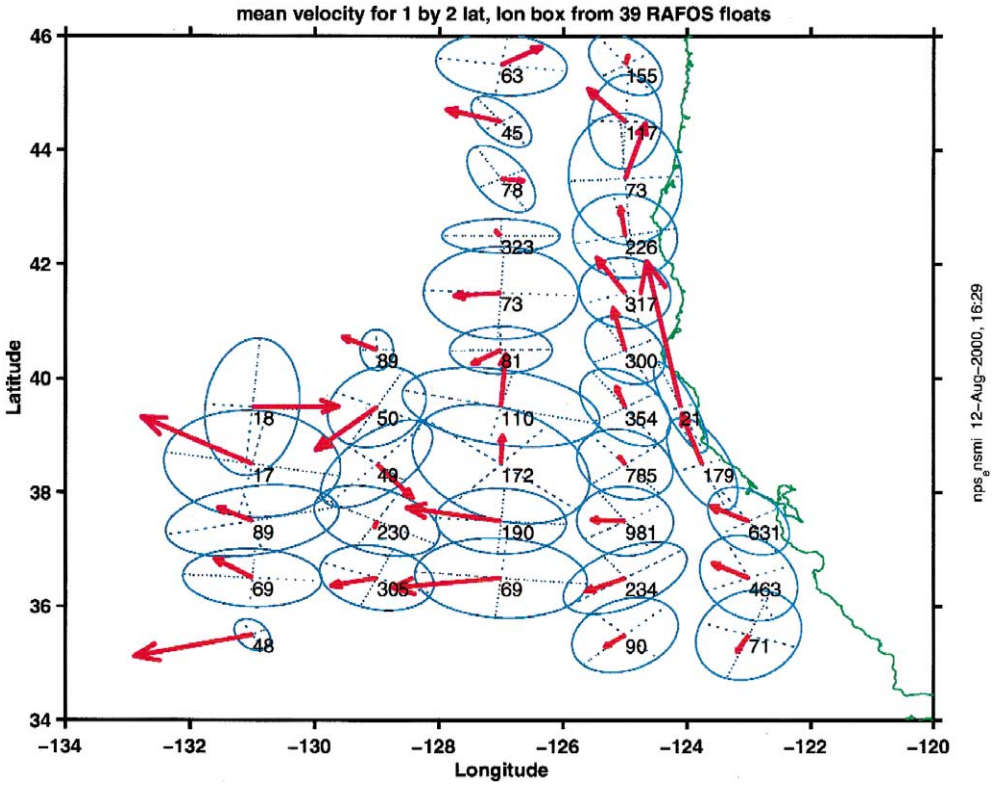

Fig. 6. Eulerian mean velocity and variance ellipses for one degree latitude by two degree longitude boxes for the RAFOS floats. The number of observations is given for each box.

low mean flow with isotropic variance. Further offshore, the mean flow is westward with the variance ellipse rotated into the east–west direction. Part of this interior distribution results from the bias of float launches. Because the floats were launched along the eastern boundary, there are no floats that can record a mean eastward motion.

2.4. Lagrangian flow patterns

Float trajectories and statistics were obtained from the interpolated and smoothed data. The observed flow patterns reinforce the observations reported by GCPC99. Continuity of the California Undercurrent, slow and reversing parallel flow just west of the continental margin, and westward flow of eddies in the ocean interior continue to be the patterns observed in the float trajectories (Fig. 5). As in GCPC99, most floats exhibited more than one of these flow types, and defining the transition from one type to another was done qualitatively, not quantitatively, based on the general characteristics of the flow.

2.4.1. California Undercurrent

Twelve floats were transported by the California Undercurrent (Table 2). Float 48 was the most remarkable, remaining with the California Undercurrent for 400 days and traveling 1530 km poleward to surface west of Vancouver Island. Twice the float appeared to have left the Undercurrent, either stalled or trapped in eddies, but after both events resumed its poleward motion with the California Undercurrent. The minimum time in the California Undercurrent was 27 days for Float 4. The median distance that floats were transported poleward was 440 km. Once a float entered the California Undercurrent, it moved poleward and seldom returned to the south in the marginal flow regime. Instead, once ejected from the California Undercurrent, a float tended to flow westward, usually exhibiting cycloidal eddy flow.

The depth distribution of the 12 California Undercurrent floats allows an estimate of the vertical shear in the California Undercurrent (Fig. 7). The floats were not synoptic; however, the variance associated with each float suggests that the vertical gradient is a good representation of the subsurface shear of the poleward current. Float 48 is the one outlier, most probably the result of the two times the float stalled. In the depth interval of the floats (135–520 m) the depth dependence of the Undercurrent horizontal speed is $S = -0.022\ (\text{cm s}^{-1}/\text{dbar}) \times \text{depth} + 18\ (\text{cm s}^{-1})$, where depth is in meters or decibars and the resultant speed is in cm s^{-1}. This shear estimate is for depths below the California Undercurrent speed maximum (Collins et al., 2000).

2.4.2. Marginal flow

Fifteen floats exhibited the flow characteristic originally labeled “marginal” flow by GCPC99. In

Table 2
The transit dates, alongshore distance, and mean and standard deviation of the depth and speed for the 12 float segments within the Undercurrent

Float	Start date	Days in current	Alongshore distance (km)	Depth (dbar)	Speed (cm s^{-1})
4	5 Sep 1993	27	286	242 ± 4	13.0 ± 5.1
5	8 Jul 1993	34	435	135 ± 14	16.3 ± 5.2
8	5 Sep 1993	43	410	302 ± 12	11.4 ± 5.2
19	26 Apr 1994	55	454	430 ± 7	10.1 ± 4.4
26	28 Sep 1994	52	480	314 ± 7	12.5 ± 3.6
28	06 Sep 1994	50	457	357 ± 9	11.6 ± 4.8
39	05 Aug 1996	136	700	513 ± 14	7.0 ± 5.6
48	05 Sept 1996	399	1530	316 ± 44	6.3 ± 4.0
50	29 Aug 1996	70	515	360 ± 9.8	9.9 ± 4.6
51	27 Feb 1997	30	167	414 ± 8.3	7.3 ± 5.4
53	20 Sep 1997	38	376	378 ± 2.2	12.4 ± 1.9
55	15 Sep 1997	46	342	364 ± 2.5	9.0 ± 2.1

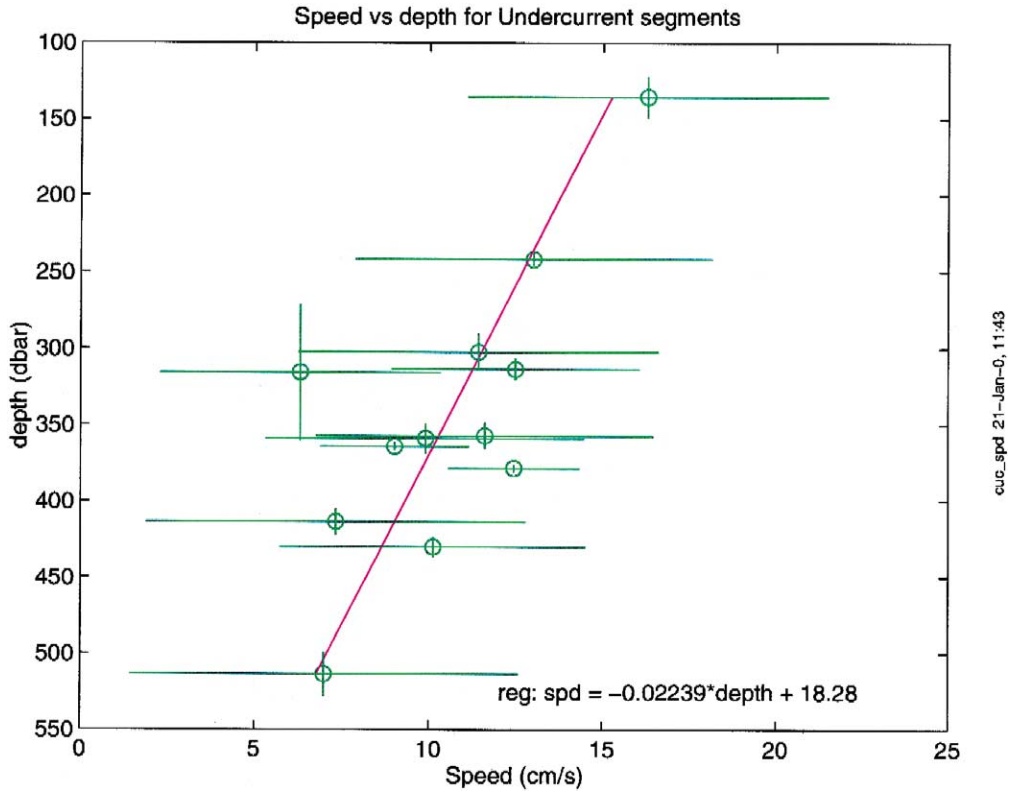

Fig. 7. Plot of the mean speed of RAFOS floats in the California Undercurrent vs. the mean float depth. A linear regression of the 12 floats gives a depth related speed of the Undercurrent of speed (cm s^{-1}) = -0.022 (cm s^{-1}/dbar) × depth + 18 (cm s^{-1}), where depth is in meters or decibars.

this mode, floats tended to move slowly parallel to the continental slope in both the poleward and equatorward directions. The average speed of these floats, 3.6 cm s^{-1}, was the lowest mean speed (by a factor of two) of all the observed float motions (Table 1). Marginal flow was only observed between Cape San Martin and Point Arena because all the float launches occurred in this region. These floats ended their subsurface missions while either still exhibiting marginal flow or moving into the California Undercurrent. It is interesting that none of the floats with marginal flow became entrained in the westward moving eddies without first being entrained by the California Undercurrent.

2.4.3. Interior flow

The floats transported away from the continental margin experienced primarily rotational flow in eddies that were translating slowly westward (Table 3). The primary difference between the original (GCPC99) and updated observations of interior flow is that more larger eddies have been sampled in recent years. GCPC99 found that most of the floats were caught in small, rapidly rotating eddies which GCPC99 characterized as submesoscale coherent vortices. Only one of the first set of floats had a radius of motion greater than 35 km. Float observations obtained since 1995 sampled a wider range of radii of motion, between 18 and 127 km, and a wider range of rotational periods. Six of the eight interior float segments had a radius of motion greater than 50 km. In addition, two floats had cyclonic rotation vs. 18 floats with anticyclonic rotation. As seen in Fig. 5, most of the interior floats were undergoing cycloidal motion at the end of the submerged missions.

The cycloidal translation and rotation of the interior float trajectories were separated using a least

Table 3
Eddy kinematics for strongly rotational float segments in both the Undercurrent and the ocean interior. %U and %V are the percentages of the observed U and V velocity components, respectively, accounted for by the combination of rotation and eddy translation

Float	Date	Long	Lat	U and V (cm s^{-1})	Radius (km)	Period (days)	Vorticity ($s^{-1} \times 10^5$)	%U and %V
4	4 Dec 1993	130.3°W	39.1°N	−2.15, −0.19	69.8	35.7	−0.41	99.4, 98.9
5	12 Aug 1993	125.3°W	42.2°N	−0.83, 0.58	17.4	10.8	−1.36	90.1, 88.9
6, 11, 13	3 Dec 1993	124.6°W	37.8°N	−0.86, −0.72	25.8	24.5	−0.61	83.6, 72.8
11	10 Jan 1994	125.5°W	37.5°N	−0.98, −0.87	18.0	17.7	−0.84	96.9, 97.4
7	27 Jul 1993	125.4°W	37.2°N	−2.40, −0.04	23.1	11.9	−1.23	92.6, 93.4
8	19 Oct 1993	125.0°W	41.6°N	−0.61, 3.05	29.5	21.0	−0.71	94.9, 92.5
10	16 Dec 1993	125.7°W	38.2°N	−1.23, 2.63	17.1	22.8	−0.64	99.3, 99.3
14	30 Jan 1994	124.6°W	38.2°N	−0.99, 0.47	26.5	24.2	−0.61	97.5, 98.5
19	7 Jun 1994	126.4°W	41.6°N	−2.25, −0.68	26.2	16.6	−0.90	92.9, 75.6
26	14 Nov 1994	124.3°W	39.0°N	−4.71, 1.21	27.9	13.7	−1.07	84.0, 83.1
28	23 Nov 1994	125.3°W	41.1°N	−2.49, 3.39	33.8	15.6	−0.93	94.9, 93.8
31	31 Aug 1994	126.3°W	38.7°N	−1.50, −1.53	73.2	27.3	−0.55	99.0, 98.5
43	21 Sep 1995	128.0°W	36.8°N	−2.01, −0.04	67.2	55.7	0.26	74.4, 68.2
29	24 Dec 1995	124.6°W	35.6°N	−5.91, 2.37	64.4	34.7	−0.46	82.5, 85.1
42	25 Aug 1996	125.8°W	37.7°N	−0.94, 0.23	89.1	59.6	−0.25	77.0, 71.7
37	10 Apr 1997	124.3°W	37.2°N	−3.09, −2.99	49.9	16.6	−0.89	95.2, 94.8
51	5 Jun 1997	128.5°W	37.0°N	−1.68, −0.40	113.0	90.6	−0.16	71.9, 73.0
32	11 Jun 1997	128.6°W	37.2°N	−1.61, −0.68	127.6	101.2	−0.15	86.9, 79.2
39	21 Jun 1997	125.5°W	45.0°N	−0.94, 0.23	46.8	63.2	−0.24	86.5, 68.8
15	27 Nov 1997	125.3°W	38.6°N	−3.44, −0.01	18.6	16.1	0.91	87.0, 70.8

squares technique (Sanderson, 1995) (Table 3). The U and V velocity components represent the translation of the eddy motion, while the period and radius define the rotational movement. %U and %V represent the percentage of the float motion that can be accounted for with the least squares technique. Lower percentages occur for floats that had only limited cycloidal motion. Fig. 8 shows the mean translation of the eddies. Except for the floats still in the California Undercurrent while undergoing cycloidal movement (floats 5, 8, and 28), the eddies moved primarily westward with a mean translation of 2.5 cm s^{-1}.

Table 3 suggests two size classes of eddy motion. One class derives from the 11 float segments showing small eddies of radius < 35 km and period < 27 days; the second class derives from the eight floats with radius of motion > 50 km and periods varying between 15 and 130 days. The question remains whether the radius of float motion can be used as a measure of the eddy size.

To date, the supporting evidence for distinguishing classes of subsurface eddies is relatively sparse. Most observations do confirm the large eddies (Huyer et al., 1998; Chereskin et al., 2000). Huyer et al. concluded that the large eddies most probably form over the continental margin through baroclinic instability. Brink et al. (2000) reached a similar conclusion for large eddies measured with surface drifters. The smaller, quicker rotating eddies, the cuddies, have proved more elusive to sample.

Huyer et al. (1998) did observe the eddy which transported float nps#7 (GCPC99). This float had a radius of motion (23.1 km) near the median (26.3 km) of the 12 eddies sampled by RAFOS floats, but with a period (11.9 days), much shorter than the median (18 days). Huyer et al. may have sampled part of this same eddy. They suggest it was half of a cyclone/anticyclone pair with weak spiciness signatures. The anticyclone was not well enough resolved to determine its size or to speculate on its formation mechanism.

2.5. Lagrangian statistics

Lagrangian single particle statistics for estimation of the decorrelation time and space scales and the rate of mixing were computed using the techniques

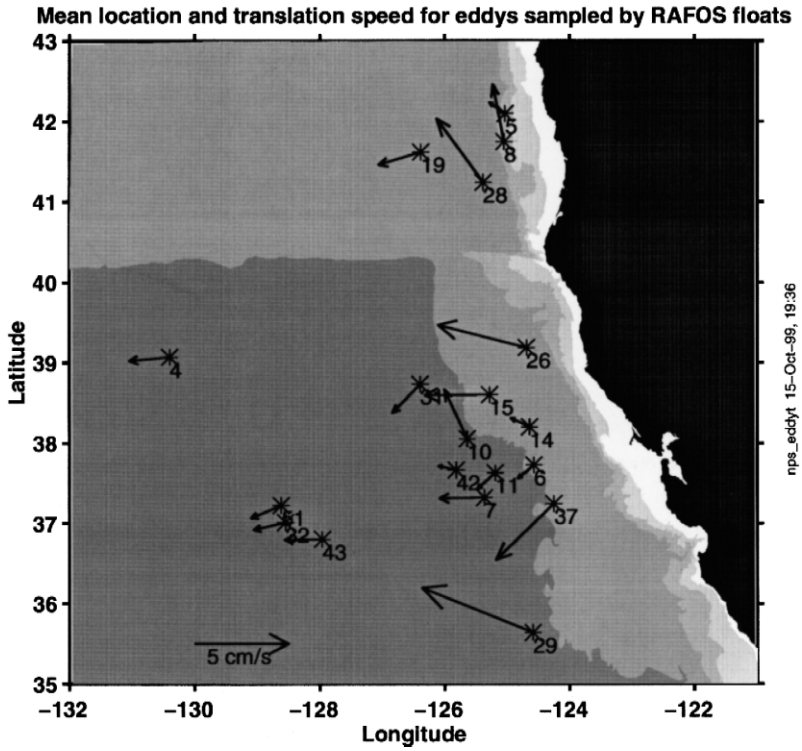

Fig. 8. The mean trajectory of each eddy sampled by the NPS RAFOS floats. The number at the base of each vector is the first float to encounter the eddy. The origin of each vector is the location where the eddy was first encountered.

summarized by GCPC99. Single particle statistical methods (Taylor, 1921) have been adapted for oceanographic application by a series of papers which are summarized in GCPC99. As before, we acknowledge that the statistics are biased because our floats were launched from a relatively fixed position on the eastern side of the ocean basin. To accomplish a truly statistical experiment would require far more floats than is financially realistic. Our experiment was designed to test the hypothesis of the continuity of the California Undercurrent. Computation of Lagrangian statistics does have a built-in bias due to this objective; however, this set of subsurface float data is the largest subsurface Lagrangian data set for

Table 4
Estimation of the Lagrangian time, space and diffusions scales from the Lagrangian autocorrelation function

Flow region	Numbers of		Time scales (days)		Length scales (km)		Diffusivity ($m^2\ s^{-1}$)	
	Floats	Psuedo	U	V	U	V	K_{uu}	K_{vv}
RAFOS floats								
All flts	38	736	6.7 ± 2.8	7.1 ± 2.6	27.2 ± 19.9	25.0 ± 12.9	1495 ± 1691	1095 ± 1044
Undercurr	12	74	5.0 ± 2.8	6.3 ± 2.7	11.4 ± 6.1	21.5 ± 14.4	308 ± 211	873 ± 908
Interior	30	425	6.8 ± 3.3	6.6 ± 2.7	31.3 ± 22.2	24.3 ± 13.1	1827 ± 1766	1151 ± 1173
Marginal	15	153	6.6 ± 1.8	7.9 ± 2.7	13.1 ± 7.5	19.4 ± 6.59	350 ± 475	546 ± 322
Model floats								
All	400	–	35.1 ± 21.3	43.8 ± 13.4	35.0 ± 26.9	66.1 ± 22.4	351 ± 294	1125 ± 541
Undercurr	259	–	27.8 ± 12.8	39.9 ± 12.3	24.2 ± 12.4	63.5 ± 22.8	235 ± 154	1144 ± 596
Interior	141	–	48.5 ± 26.6	51.1 ± 12.3	54.5 ± 34.2	70.7 ± 20.7	563 ± 359	1103 ± 415

an eastern boundary anywhere in the world. For this reason, it is appropriate to compute the statistics and to compare them with other published Lagrangian values.

Lagrangian statistics for the entire data set, including the pseudo floats, and the different flow regimes are presented in Table 4. The reason that the sum of the pseudo floats for the three flow regimes does not match the number (736) for the full set is because some pseudo floats, in dividing the float observations into the three regimes, end up with less than the required 20 days.

The Lagrangian time scales are similar for the whole set and the three flow types. The California Undercurrent had the shortest time scales; however, they are all similar. The decorrelation length scales are likewise similar except for the *U* component of the Undercurrent flow. This probably arises from floats that end their California Undercurrent motion by moving westward into the ocean interior. The low diffusion of the California Undercurrent is most probably related to its jet-like nature and the arbitrary ending of Undercurrent segments when the float moves offshore.

3. Model floats

The model results used here are from a run of the Parallel Ocean Program (POP) to simulate a 5-year period. The model was forced using European Centre for Medium-Range Weather Forecasts (ECMWF)

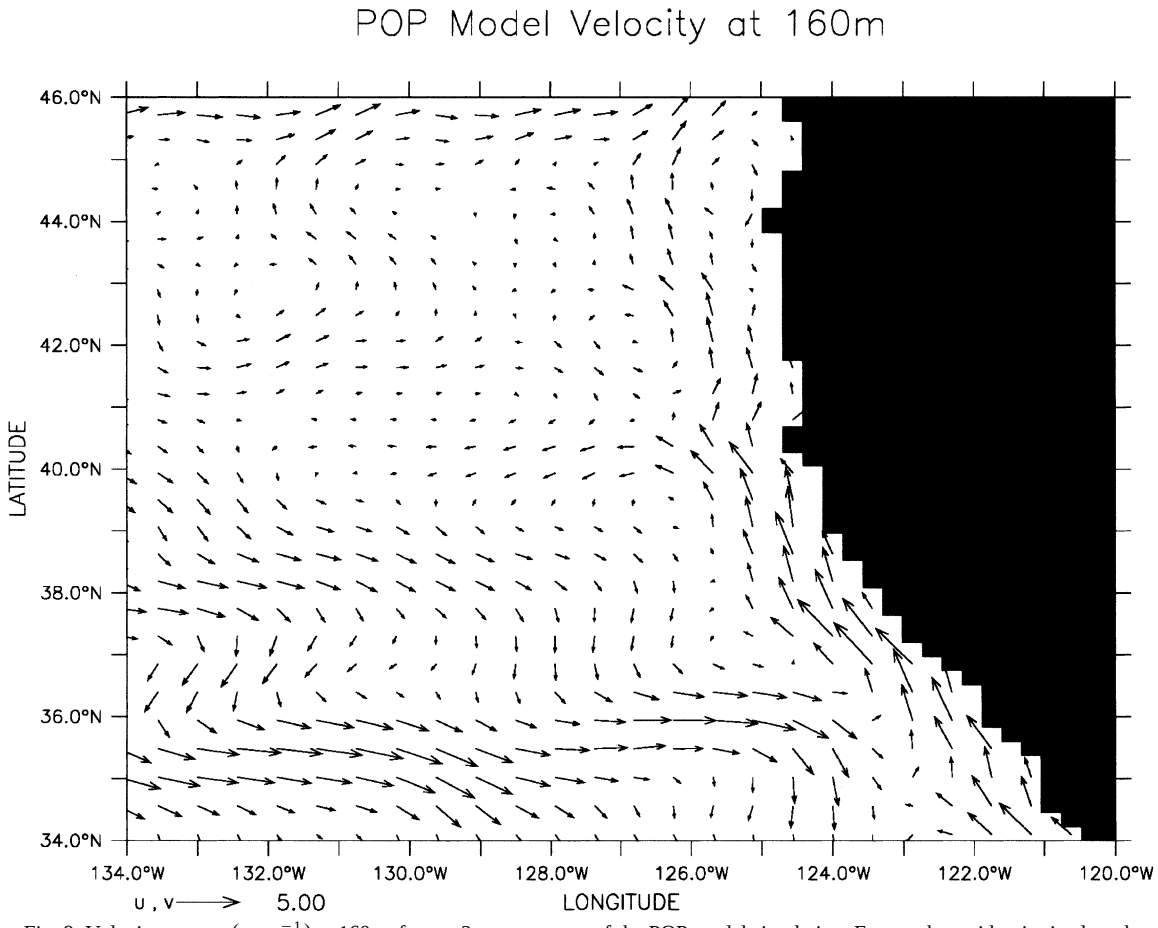

Fig. 9. Velocity vectors (cm s^{-1}) at 160 m from a 2-year average of the POP model simulation. Every other grid point is plotted.

winds, Barnier et al. (1995) surface heat flux, and Levitus (1982) surface salinity restoring on an almost global Mercator grid (78°S to 78°N) with horizontal resolution of 0.28° at the equator (0.06° at 78°S and 78°N) and 20 vertical levels. The model setup is essentially the same as run POP11 as described by Maltrud et al. (1998) with one difference: instead of 3-day ECMWF winds, this run uses daily ECMWF winds for the period 1993–1997.

Qualitatively the model is able to reproduce the major components of the California Current System. The simulated California Current is a narrow, meandering surface current typically located several hundred kilometers offshore. In winter a poleward surface inshore current appears that resembles the Davidson Current. The model California Undercurrent is a very persistent feature (especially south of Cape Mendocino) located over the continental slope with its core between 150 and 200 m below the surface (Figs. 9 and 10).

As is typical for this and other models with similar resolution, the current velocities are too small. For example, the simulated California Current has maximum instantaneous speeds on the order of 20 cm s^{-1} and maximum (Eulerian) mean speeds near 10 cm s^{-1}, both of which are a factor of 3 to 4 too low (e.g. Brink et al., 2000). In addition to weak mean flow, the variability, both on a global basis and in this particular area, is also too low in this model. Averaged over the California Current region, the

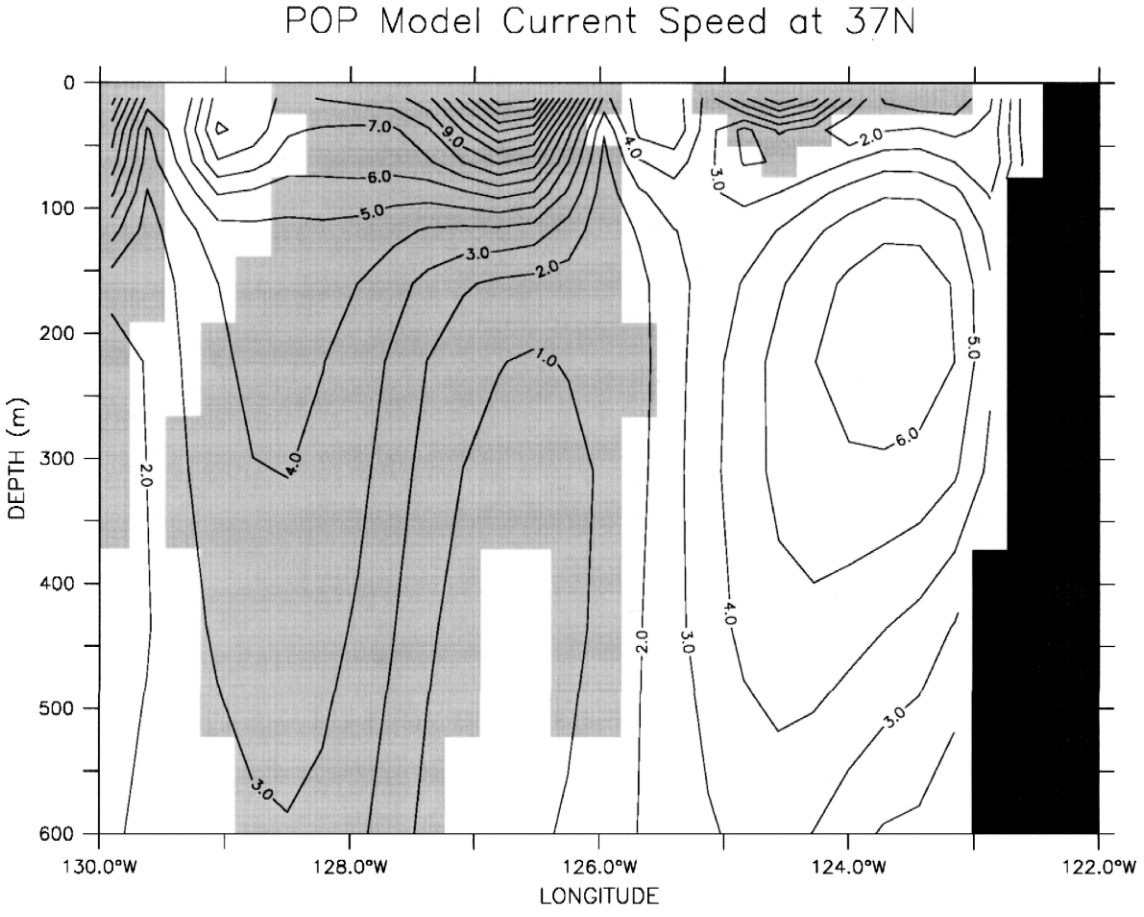

Fig. 10. Instantaneous cross section of current velocity (cm s^{-1}) contours at 37°N from the POP model. Grey background denotes southward flow (as in the surface California Current) and white background denotes northward flow (as in the California Undercurrent).

model surface height variability is about 50% of the value given by blended TOPEX-ERS1 data (Le Traon and Ogor, 1998; Le Traon et al., 1998). Worse still, the near surface eddy kinetic energy is low by almost an order of magnitude compared to estimates based on drifter, altimeter and ADCP data (Kelly et al., 1998).

3.1. Model floats

The model floats are massless particles that are advected every time step with the local three-dimensional velocity linearly interpolated to the float position. They are neither isobaric nor isopycnal. More details can be found in Maltrud et al. (1998). For the current run, 20 deployments were made from the same start positions as for the true RAFOS floats. Each deployment was separated by 20 days so that particle release times occurred during all seasons. The float positions were sampled once per day and written to a file along with the local values of the velocity, potential temperature, and salinity.

Trajectories of the model floats exhibit the same flow regimes as the RAFOS floats: some stay in the undercurrent, while others depart into the interior (Fig. 11). One noticeable difference is southeastward flow well offshore that is associated with the eastern edge of the model's subtropical gyre, but that is not seen in any of the real floats. In addition, there is only a minimal signature of flow along the continental margin, likely due to the grid resolution. As a consequence, the model floats were separated into only two groups for this analysis (Table 1): those that remain in the California Undercurrent essentially all their lifetimes (259 total floats), and those that penetrate into the interior (141 floats). Because of the large number of floats, no attempt was made to split the float trajectories for separate analyses of the Undercurrent and interior portions of those trajectories exhibiting both types of flow. Consequently, the interior float statistics will have contributions from the times they spent in the California Undercurrent. Also, because of the large number of floats, no "pseudo" floats were created using the model floats.

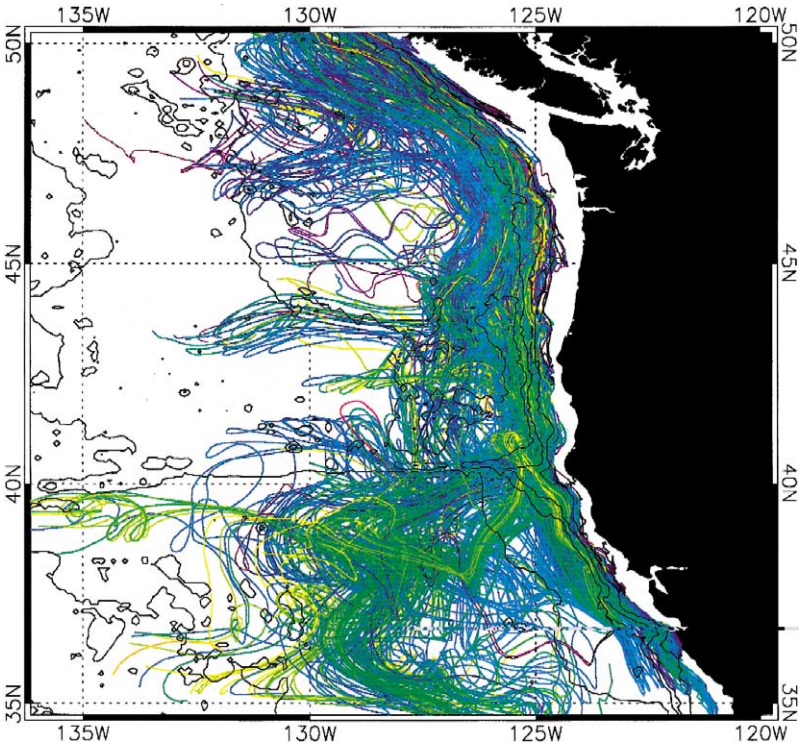

Fig. 11. Ensemble spaghetti diagram for the Lagrangian particle drifters in the POP model.

The sample size is reasonably large as it is. Another important difference in the model analysis is that the trajectories vary from three to four years long.

Close inspection of the model trajectories that enter the interior shows that none of the particles appear to have been trapped by eddies. There are occasional single loops in the paths (which can be seen in the data), but no persistent cycloidal motion. Instead, the model floats typically move offshore in fairly smooth coherent jets. This is not consistent with the real floats, where most that enter the interior are carried there by eddies. While the model certainly cannot resolve submesoscale motions, it does exhibit subsurface mesoscale eddies in this region, although they are less energetic and fewer than in the real ocean. Unfortunately, none of the model floats sampled these eddies.

Tables 1 and 4 show the same Lagrangian statistics derived for the model floats as were computed for the real floats. As with the surface current, we see that mean subsurface velocities are typically a factor of 3 to 5 too small. Figs. 7 and 12 reveal the difference in the California Undercurrent vertical shear observed by the real floats and the model floats, respectively. Since the model particles are velocity tracers and can change depth easily, the vertical shear of the horizontal velocity was computed by binning the particle data by depth rather than by averaging each individual float during its California Undercurrent excursion. As expected, the shear is quite low (due to the low velocity), although the nondimensional shear disagrees only by a factor of about 2. The regression computed for the range 125–475 m from these data is speed (cm s^{-1}) = -0.0024 (cm s^{-1}/dbar) × depth + 2.8 (cm s^{-1}), where depth is, again, in meters or decibars.

As a check of the Lagrangian estimate of the vertical velocity shear, an Eulerian average of the flow in the Undercurrent region was calculated. The Eulerian estimate [S (cm s^{-1}) = -0.0024 (cm

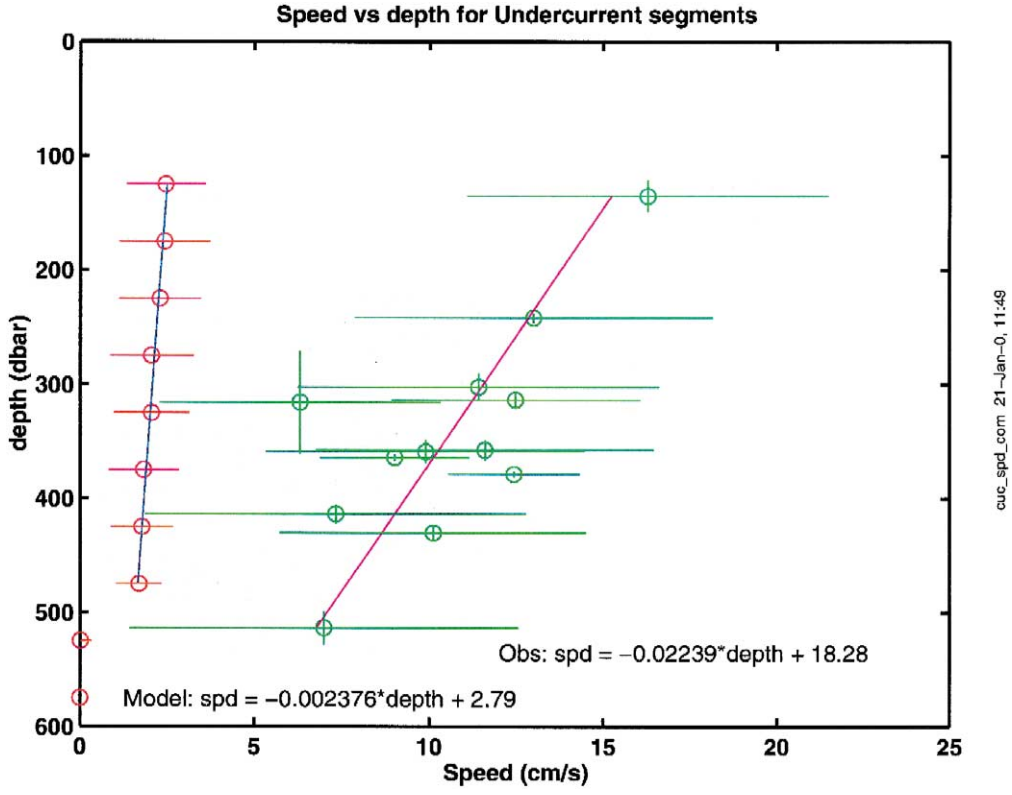

Fig. 12. The mean speed vs. depth from RAFOS and model floats for the segments. The RAFOS data are the same as in Fig. 7.

s^{-1}/dbar) × depth + 2.7 (cm s^{-1})] is very similar to the model Lagrangian estimate, thus confirming that while the model underestimates the velocity, it does reproduce sheared flow.

In the California Undercurrent, the ratio U/V is about the same for both model and RAFOS data, reflecting the jet-like nature of the flow. In the interior the mean model speed is about the same as the model Undercurrent speed while the model mean U and V are statistically indistinguishable from zero. Note also that the velocity variability (as measured by the standard deviation) is also much smaller for the model floats not only in absolute magnitude, but also as compared to the mean.

The Lagrangian time scales computed from the autocorrelation function (Table 4) for the model floats are also different from the real floats by a factor of about five, being on the order of a month instead of a week. Both Lagrangian and Eulerian energy spectra of the velocity fluctuations (not shown) confirm that there is very little energy in the flow for periods less than about 30 days. It is unclear why the model is so deficient at submonthly time scales (especially given the daily wind forcing). But it is likely that grid resolution and mixing parameters play a role. This question will have to be investigated later.

The model Lagrangian length scales are much closer to the real float values. But it is likely that this agreement is simply fortuitous, since the length scale is proportional to the integral time scale (which is too large) and the magnitude of the rms velocity fluctuations (which is too small). For the same reason, any apparent agreement of the magnitude of model diffusivities with the data is also likely to be fortuitous. However, it is interesting to note that in the Undercurrent, the meridional diffusivity is much larger than the zonal diffusivity, in agreement with the data.

4. Discussion

California Undercurrent observations made during the last few years, comprised of the Lagrangian observations reported here, a series of cross-shore ship-based ADCP absolute velocity measurements (Pierce et al., 2000), and long-term fixed observations (e.g. Collins et al., 2000), confirm the robust and permanent nature of the California Undercurrent. The high density of measurements have shown the current to exist offshore of the continental shelf break between Pt. Conception, CA, to Vancouver Island, Canada. Other shorter observations suggest that the current is a coherent feature even farther to the north and south (see GCPC99). The vertical shear of the Undercurrent velocity obtained by the floats agrees well with observations made off Pt. Sur, CA (Collins et al., 2000).

The temporal distribution of the floats, while skewed to the summer and fall months, found subsurface poleward flow during all months of the year (Fig. 4). Unfortunately the present data are still to sparse to determine possible seasonal (or annual) fluctuations. Still, these data tend to contradict the observations of seasonal reversal of the Undercurrent reported by Chelton (1984). The most likely explanation for the discrepancy is the relatively narrow width of the current. Chelton's analysis was based on the CalCOFI hydrographic data grid, which has a wide station spacing at the continental margin. In addition, the CalCOFI data were only collected between the surface and 500 dbar. It is likely that the poleward flow could not always be distinguished in the earlier data.

Because we are dealing with only subsurface data, we are unable to discuss whether what we call the California Undercurrent remains as a subsurface maximum or at times is merged with a surface flow creating a surface maximum. For clarity and lack of data we have called the subsurface poleward flow the California Undercurrent throughout. Further observations are needed to clarify whether the periods of strengthening poleward flow to the surface (Lynn and Simpson, 1987; Hickey, 1998; Reid and Schwartzlose, 1962) represent the merging of two flows, e.g. the inshore flow and the California Undercurrent, or expansion to the surface of the California Undercurrent. One way this can be addressed is with a careful analysis of the hydrographic signatures of the surface and subsurface flows during periods of both surface and subsurface flow maxima.

The transition from flow in the California Undercurrent to interior flow is another area needing further investigation. The large range in size of the rotational radii from the float trajectories suggests eddies of many different sizes. One question that is

not resolved in these data is the size of the eddies sampled by the floats. However, assuming solid body rotation of the floats, there appear to be at least two classes of eddies associated with the California Undercurrent. The smaller and more rapidly rotating eddies are the submesoscale coherent vortices, which GCPC99 termed "cuddies" for California eddies. They argued that these small eddies were subsurface features most likely caused by frictionally induced reduction of the vorticity in the Undercurrent. Steger et al. (2000) reported a large ageostrophic current along the continental margin when geostrophic currents from hydrographic data were compared to ship-mounted ADCP measurements. Huyer et al. (1998) found subsurface lenses of California Undercurrent water in the ocean interior associated with large subsurface eddies.

The larger eddy motion, typified by large radius (>50 km) and period generally greater than 30 days, is due to other processes. Large mesoscale eddies extending from the surface to below 1000 m most likely form through baroclinic instability (Huyer et al., 1998; Brink et al., 2000). This range of eddy motion clearly shows the dynamic nature of the eastern boundary region.

The Lagrangian statistics for floats in the interior compare well to other published values for the northeast Pacific (Table 5). In general, the subsurface RAFOS floats (GCPC99 and this study) have slightly longer time, but have similar length, scales and diffusivities. The new estimates of the time and length scales are larger than determined in GCPC99, which is probably due to the sampling of a greater number of larger eddies. Similarly, the new diffusivity estimates are lower, again probably due to transport in the larger, slower eddies. Comparison of GCPC99 and the new estimates also indicates that the sample size remains marginal in terms of computing robust Lagrangian statistics.

While the POP model simulation does exhibit the major circulation features of the California Current System, both the mean and fluctuational energies were found to be quite low compared to those from observations. The main reason is the model resolution which is considered to be in the "eddy-permitting" regime since the grid spacing (≈ 25 km) is comparable to the deformation radius in this region. A regional model study by Batteen (1997) that had similar model physics and wind forcing, but had no bathymetry and a threefold finer offshore spatial resolution, achieved results closer to the observations. Both the surface and subsurface currents are stronger, with instantaneous maximum speeds in the Undercurrent greater than 20 cm s^{-1} in Batteen's (1997) model vs. only about 10 cm s^{-1} in POP, 18 cm s^{-1} from RAFOS and greater than 25 cm s^{-1} from ADCP (Pierce et al., 2000). In addition, the width of the undercurrent in Batteen's model is less than 100 km vs. a width greater than 200 km in POP, but less than 50 km from observations (Pierce et al., 2000). It is interesting to note, however, that the model volume transport in the 125–325 m depth range is about 1 Sv (1×10^6 m^3 s^{-1}), which agrees well with estimates based on ADCP data (Pierce et al., 2000). Thus, the model increase in cross-sectional area compensates for the low model velocity

Table 5
Comparison of interior single particle statistics with other eastern Pacific Lagrangian estimates

Authors	Diffusivity (m^2 s^{-1})		Time scales (days)		Length scales (km)	
	K_{uu}	K_{vv}	U	V	U	V
Subsurface						
Present results	1827	1151	6.8	6.6	31	24
Garfield et al. (1999)	1970	1830	4.4	4.0	25	23
Thomson et al. (1990)	1700	2200	2.6	2.7	20	23
Surface						
Poulain and Niiler (1989)	3400	4300	4.2	4.7	40	48
Brink et al. (1991)	8620	2430	3.3	0.9		
Paduan and Niiler (1993)	835	1524	2.8	3.8	13.9	22.0
Swenson and Niiler (1996)	4200	4500	2.9	3.5	32	38

and results in a volume transport that matches that from observations.

Comparison of Lagrangian statistics from the model with those from the RAFOS floats also highlights the effect of model resolution. Numerical diffusion drastically reduces the small scale energy, resulting in a poor representation of the Lagrangian autocorrelation function. Thus, the statistical values derived from this function don't agree well on a term by term basis with those derived from the RAFOS data. However, the fact that both the meridional length scale and diffusivity are greater than their zonal counterparts in the Undercurrent is a significant point of agreement between the model and data statistics, implying that the model floats are constrained to remain near the coast.

Although model deficiencies degrade the ability to make satisfactory quantitative comparisons with the RAFOS data, the two sets of trajectories have many important characteristics in common. In particular, both show a continuous undercurrent and westward flow into the ocean interior, especially south of Cape Mendocino, but also in the vicinity of Cape Blanco and near 45°N. What is missing from the model trajectories are submesoscale motions that cannot be resolved, and entrapment in sporadic mesoscale eddies. It is likely that the latter problem is in part due to the excessive width of the model undercurrent. Since the simulated current is typically about 200 km wide, the deployments were made on the inshore edge, making it less likely that they would end up in an eddy that forms on the offshore side of the current. In future studies of this sort, in order to get better sampling it may be worthwhile to depart from the requirement that the model floats be deployed at the same locations as the real floats.

5. Conclusion

The major objectives of this paper were to report on the expanded set of RAFOS subsurface Lagrangian drifters for the northeast Pacific and to provide a comparison of the float observations with Lagrangian flow from a global high resolution model. The new float data confirm the earlier assessment of GCPC99. None of the earlier observations were changed significantly; rather the confidence in the observations has improved. The poleward flow of the California Undercurrent appears to be a permanent feature, not a seasonally reversing flow as observed at the surface. Eddy motion continues to be the primary mechanism by which water transported poleward by the Undercurrent is transported into the ocean interior.

Comparison between the RAFOS observations and massless particles tracked in the POP model simulation has shown that the model can capture the major large scale Lagrangian circulation features of the California Current System. However, both the mean and eddy energies in this region are substantially deficient, with the latter resulting in poor model estimates of the Lagrangian time and space scales. Model resolution is certainly responsible for much of the problem, although other model deficiencies (such as subgrid-scale parameterizations and mixed layer physics) may also be playing a role. Recent POP simulations of the North Atlantic (Smith et al., 2000) have shown substantial improvement in both the mean flow and eddy variability as the resolution reaches 0.1°. The California Current System will be a significant point of comparison for upcoming 0.1° global ocean simulations. This study helps lay the groundwork for just such a comparison.

Acknowledgements

The POP model simulations were supported by the DOE Climate Change Prediction Program. The RAFOS program has been supported by the Naval Postgraduate School, the Oceanographer of the Navy and the Office of Naval Research. A project of this size obviously depends on many more people than the authorship of this paper. Pierre Tilliet has kindly accommodated some interesting suggestions on the floats. Andy Anderson has helped with float preparation. Kirk Kingsbury, director of the NCEL pressure facility, continues to make the float ballasting a successful endeavor. Julie McClean initiated the discussion which led to the comparison of the RAFOS floats with the POP model. We thank the thoughtful reviewers, whose comments substantially improved the manuscript.

References

Barnier, B., Siefridt, L., Marchesiello, P., 1995. Thermal forcing for a global ocean circulation model using a three-year climatology of ECMWF analyses. J. Mar. Syst. 6, 363–380.

Batteen, M.L., 1997. Wind-forced modeling studies of currents, meanders, and eddies in the California Current system. J. Geophys. Res. 102 (C1), 985–1010.

Brink, K.H., Beardsley, R.C., Niiler, P.P., Abbot, M., Huyer, A., Ramp, S., Stanton, T., Stuart, D., 1991. Statistical properties of near-surface flow in the California coastal transition zone. J. Geophys. Res. 96 (C8), 14693–14706.

Brink, K.H., Beardsley, R.C., Paduan, J., Limeburner, R., Caruso, M., Sires, J.G., 2000. A view of the 1993–1994 California Current based on surface drifters, floats, and remotely sensed data. J. Geophys. Res. 105 (C4), 8575–8604.

Chelton, D., 1984. Seasonal variability of alongshore geostrophic velocity off central California. J. Geophys. Res. 89, 3473–3486.

Chereskin, T.K., Morris, M.Y., Niiler, P.P., Kosro, P.M., Smith, R.L., Ramp, S.R., Collins, C.A., Musgrave, D., 2000. Spatial and temporal characteristics of the mesoscale circulation of the California Current from eddy-resolving moored and shipboard measurements. J. Geophys. Res. 105, 1245–1269.

Collins, C.A., Garfield, N., Rago, T.A., Rischmiller, F.W., Carter, E., 2000. Mean structure of the inshore countercurrent and California Undercurrent off Pt. Sur, California. Deep-Sea Res. 47 (5–6), 765–782.

Garfield, N., Collins, C.A., Paquette, R.G., Carter, E., 1999. Lagrangian exploration of the California Undercurrent, 1992–95. J. Phys. Oceanogr. 29 (4), 560–583.

Hickey, B., 1998. Coastal oceanography of western North America from the tip of Baja California to Vancouver Island. In: Robinson, A.R., Brink, K.H. (Eds.), The Global Coastal Ocean Regional Studies and Syntheses. The Sea, vol. 11, Wiley, New York, pp. 345–393.

Huyer, A., Barth, J.A., Kosro, P.M., Shearman, R.K., Smith, R.L., 1998. Upper-ocean water mass characteristics of the California Current, Summer 1993. Deep-Sea Res. 45, 1411–1442.

Johnson, R.H., Norris, R.A., 1968. Geographic variation of SOFAR speed and axis depth in the Pacific Ocean. J. Geophys. Res. 73 (14), 4695–4700.

Kelly, K.A., Beardsley, R.C., Limeburner, R., Brink, K.H., Paduan, J., Chereskin, T.K., 1998. Variability in the near-surface eddy kinetic energy in the California Current based on altimetric, drifter, and moored current data. J. Geophys. Res. 103 (C6), 13067–13083.

Le Traon, P.Y., Ogor, F., 1998. ERS-1/2 orbit error improvement using TOPEX/POSEIDON: the 2 cm challenge. J. Geophys. Res. 103, 8045–8057.

Le Traon, P.Y., Nadal, F., Ducet, N., 1998. An improved mapping method of multi-satellite altimeter data. J. Atmos. Oceanic Technol. 15, 522–534.

Levitus, S., 1982. Climatological Atlas of the World Oceans. NOAA Prof. Paper 13, U.S. Govt. Printing Office, Washington, DC.

Lupton, J.E., Baker, E.T., Garfield, N., Massoth, G., Feely, R., Cowen, J., Greene, R., Rago, T.A., 1998. Tracking the evolution of a hydrothermal event plume using a RAFOS neutrally buoyant drifter. Science 280, 1052–1055.

Lynn, R.J., Simpson, J.J., 1987. The California Current System: the seasonal variability of its physical characteristics. J. Geophys. Res. 92, 12947–12966.

Maltrud, M.E., Smith, R.D., Semtner, A.J., Malone, R.C., 1998. Global eddy-resolving ocean simulations driven by the 1985–1995 atmospheric winds. J. Geophys. Res. 103 (C13), 30825–30853.

Paduan, J.D., Niiler, P.P., 1993. Structure of velocity and temperature in the northeast Pacific as measured with Lagrangian drifters in fall 1987. J. Phys. Oceanogr. 23, 1709–1720.

Paquette, R.G., 1996. RAFOS Float Manual. Naval Postgraduate School, Monterey, CA, 44 pp. [Available from Department of Oceanography, Naval Postgraduate School, 833 Dyer Rd., RM 328, Monterey, CA 93943.].

Pierce, S.D., Smith, R.L., Kosro, P.M., Barth, J.A., Wilson, C.D., 2000. Continuity of the poleward undercurrent along the eastern boundary of the mid-latitude north Pacific. Deep-Sea. Res., Part II, 47, 811–829.

Poulain, P.-M., Niiler, P.P., 1989. Statistical analysis of the surface circulation in the California Current System using satellite-tracked drifters. J. Phys. Oceanogr. 19, 1588–1603.

Reid, J.L., Swartzlose, R.A., 1962. Direct measurements of the Davidson Current off Central California. J. Geophys. Res. 67 (6), 2491–2497.

Rischmiller, F.W., 1993. Variability of the California Current System off Point Sur, California, from April 1988 to December 1990. MS thesis, Department of Oceanography, Naval Postgraduate School, Monterey, CA, 159 pp. [Available from Department of Oceanography, Naval Postgraduate School, 833 Dyer Rd., RM 328, Monterey, CA 93943.].

Rossby, T., Dorson, D., Fontaine, J., 1986. The RAFOS System. J. Atmos. Oceanic Technol. 4, 672–679.

Sanderson, B.G., 1995. Structure of an eddy measured with drifters. J. Geophys. Res. 100, 6761–6776.

Schwing, F.B., Husby, D.M., Garfield, N., Tracy, D.E., 1991. Mesoscale response of coastal waters off Central California to wind events following the Spring 1989 transition: analysis of CTD surveys and AVHRR imagery. Calif. Coop. Oceanic Fish. Invest. Rep. 32, 47–62.

Smith, R.D., Maltrud, M.E., Bryan, F.O., Hecht, M.W., 2000. Numerical simulation of the North Atlantic Ocean at 1/10°. J. Phys. Oceanogr. 30 (7), 1532–1561.

Steger, J.M., Schwing, F.B., Collins, C.A., Rosenfeld, L.K., Garfield, N., Gezgin, E., 2000. Circulation and water masses in the Gulf of the Farallones. Deep-Sea Res. 47 (5–6), 907–946.

Swenson, M.S., Niiler, P.P., 1996. Statistical analysis of the surface circulation of the California Current. J. Geophys. Res. 101 (C10), 22631–22644.

Thomson, R.E., LeBlond, P.H., Emery, W.J., 1990. Analysis of deep-drogued satellite-tracked drifter measurements in the northeast Pacific. Atmos. Ocean 24, 409–443.

Taylor, G.I., 1921. Diffusion by continuous movements. Proc. London Math. Soc. 20, 196–212.